Modeling of the Bistatic Electromagnetic Scattering From Sea Surfaces Covered in Oil for Microwave Applications

Nicolas Pinel, Nicolas Déchamps, and Christophe Bourlier, *Associate Member, IEEE*

***Abstract*—This paper describes the influence of oil pollution over sea surfaces on the height spectrum and the height autocorrelation function of rough surfaces. An oil slick damps the capillarity waves of the surface height spectrum and reduces the root mean square slope of the surface. These modified functions then have an influence on the radar cross section (RCS) from contaminated sea surfaces. The bistatic RCS of the contaminated sea surface is then presented by comparison with a clean sea: results from a benchmark numerical model are presented and compared with a new semiempirical model using the geometric optics approximation and then the first-order smallslope approximation.**

***Index Terms*—Ocean remote sensing, radar scattering, scattering by rough surfaces, sea surface.**

I. Introduction

TO CALCULATE the electromagnetic (EM) field scattered by a single random rough interface or by a stack of random rough interfaces, two key parameters need to be known, i.e., the surface height probability density function and the height autocorrelation function, or its associated height spectrum (which is equal to the Fourier transform of the autocorrelation function). If the surface is assumed to be stationary (spatially homogeneous) and obeys Gaussian statistics (in this paper, these assumptions are used), knowledge of the height spectrum is sufficient. Moreover, the dielectric relative permittivities of considered media must be determined to resolve the raised EM problem.

For asymptotic or approximate methods valid for a single rough interface, like the Kirchhoff approximation [1] and the small perturbation method (e.g., see [2]–[5]), the two-scale model [6], the small-slope approximation (SSA) [7] (see also [8]–[11] for the specific case of a sea surface), the weighted and the local curvature approximations [12], the integral equation model and their modified versions [13], and so on (see the topical review of Elfouhaily and Guérin [14]), the surface height spectrum or the height correlation function is required for the computation of the radar cross section (RCS).

For "exact" numerical methods, one must simulate a realization of the surface heights by using, for example, a spectral method (e.g., see [15, Ch. 4]). Combined with a method of moments (e.g., see [15] for a single rough interface and [16] for a stack of two rough interfaces) and with the knowledge of the permittivities of considered media, the RCS can be computed from several independent statistical profiles.

This paper is devoted to a detailed analysis of the EM wave scattering from a sea that is covered in oil. More precisely, it focuses on the case of homogeneous oil slicks. This allows better detection of oil spills, as well as possibly an estimation of the amount of oil spilled, as the scattering coefficient depends on the layer thickness. We will study the influence of an oil film over a sea surface on the surface height spectrum and the autocorrelation function. Then, with the knowledge of the relative permittivities of the sea [17] and the oil film [18], [19], the RCS of a contaminated sea surface is compared to that of a clean sea surface. A benchmark numerical method is used based on the forward–backward (FB) method [20] for a single rough surface and the propagation inside layer expansion (PILE) method [16] combined with the FB method for the contaminated sea (i.e., a stack of two rough interfaces). A comparison with a new semiempirical model for thin layers is made based on the geometric optics approximation (GOA) and then on the first-order small slope approximation (SSA-1).

In Section II, we propose to calculate the surface height spectrum of a rough sea surface that is covered in oil (also called contaminated sea surface) S_{cont} and to compare it with that of a clean sea surface S_{clean}, which is given by the Elfouhaily *et al.* [21] model. For the contaminated sea surface, the Lombardini *et al.* [22] model is used, which does not depend on the oil film thickness. In addition, from S_{cont}, we compare the surface height correlations of the clean and the contaminated rough seas, generate a statistical realization of the surface heights and slopes, and represent the root mean square (rms) slope required, e.g., in the GOA. Section IV is devoted to the impact of a contaminated sea surface against a clean sea surface on the bistatic RCS. Results from the benchmark numerical model are presented and compared with a new semiempirical model using the GOA and then the SSA-1.

Manuscript received March 15, 2007; revised May 4, 2007.

N. Pinel and N. Déchamps are with the Radar Team, Institut de Recherche en Electrotechnique et Electronique de Nantes Atlantique (IREENA) Laboratory, Ecole Polytechnique de l'Université d Nantes (EPUN), University of Nantes, 44306 Nantes Cedex 03, France (e-mail: nicolas.pinel@univ-nantes.fr).

C. Bourlier is with the Radar Team, Institut de Recherche en Electrotechnique et Electronique de Nantes Atlantique (IREENA) Laboratory, Ecole Polytechnique de l'Université d Nantes (EPUN), University of Nantes, 44306 Nantes Cedex 03, France, and also with the Centre National de la Recherche Scientifique (CNRS), 75794 Paris Cedex 16, France.

Color versions of one or more of the figures in this paper are available online at http://ieeexplore.ieee.org.

Digital Object Identifier 10.1109/TGRS.2007.902412

II. Roughness Spectrum of a Contaminated Sea Surface

For the sake of simplicity, we will concentrate here on the problem of 1-D surfaces; nevertheless, the extension to a 2-D case does not raise any particular problem.

Lombardini *et al.* [22] demonstrated that ripples on a water surface covered by an oil film exhibit a damping effect, which is characterized by a maximum that is located in the gravity–capillary region around the frequency $f = 10$ Hz. This damping effect is expressed by the attenuation coefficient explicitly given by [22]

$$y(f; E_0, \omega_D) = \frac{1 \pm 2\tau + 2\tau^2 - X + Y(X+\tau)}{1 \pm 2\tau + 2\tau^2 - 2X + 2X^2} \quad (1)$$

where

$$\tau = \left(\frac{\omega_D}{2\omega}\right)^{\frac{1}{2}} \quad X = \frac{E_0 k^2}{\rho(2\nu\omega^3)^{\frac{1}{2}}} \quad Y = \frac{E_0 k}{4\nu\rho\omega} \quad (2)$$

are dimensionless quantities and

$$f = \frac{\omega}{2\pi} = \frac{(\varsigma k^3/\rho + gk)^{\frac{1}{2}}}{2\pi} \quad (3)$$

is the dispersion law. E_0 denotes the elasticity modulus (in newtons per meter), $\rho = 10^3$ kg/m^3 is the water density, $\nu = 10^{-6}$ m/s^2 is the kinematic viscosity, $\varsigma = 74 \times 10^{-3}$ N/m is the surface tension, $g = 9.81$ m/s^2 is the acceleration of gravity, and k is the wavenumber. Furthermore, ω_D is a characteristic pulsation, which depends on the diffusional relaxation for soluble films and on the structural relaxation between intermolecular forces for insoluble films. Thus, y depends on the frequency f or the wavenumber k (dispersive law) and on $\{E_0, \omega_D\}$. In (1), a plus sign refers to soluble films, whereas a minus sign refers to insoluble films. In what follows, we will only concentrate on insoluble homogeneous films. The case of partially soluble films needs to be studied separately, as it implies, in general, the modeling of surface scattering, as well as volume scattering, from the oil emulsions. For the typical frequencies used here (around 3 GHz), however, the emulsion can be modeled by an effective permittivity [23]–[25]. Nevertheless, the Lombardini *et al.* model takes the solubility into account very basically, as it does not depend on the oil percentage in water–oil suspension, which is not physical. Then, the case of soluble films will not be considered further: this paper concentrates on insoluble films, which occur for slight to moderate wind speeds ($u_{10} <\sim 8$ or 10 m/s) [25].

According to Lombardini *et al.* [22], the height spectrum of a contaminated sea water S_{cont} is related to the clean sea height spectrum S_{clean} by the ratio

$$S_{\text{cont}}(k; u_{10}, \phi, E_0, \omega_D) = \frac{S_{\text{clean}}(k; u_{10}, \phi)}{y_s(k; E_0, \omega_D)} \quad (4)$$

where y_s is the damping ratio. In what follows, for the clean sea height spectrum, the sea is assumed to be fully developed, and one uses the Elfouhaily *et al.* model [21], which is defined as

$$S_{\text{clean}}(k; u_{10}, \phi) = M(k)\left[1 + \Delta(k)\cos(2\phi)\right]/(2\pi) \quad (5)$$

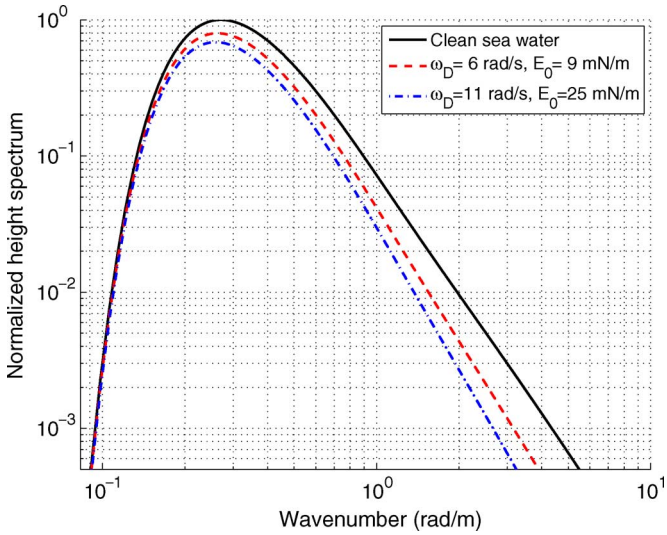

Fig. 1. Normalized height spectrum (isotropic part) of clean and contaminated sea surfaces versus the wavenumber k. The wind speed is $u_{10} = 5$ m/s.

where $M(k)$ and $\Delta(k)$ are the isotropic and anisotropic parts of the height spectrum, respectively. They depend on the wind speed u_{10} defined at 10 m above the sea. ϕ stands for the wind direction. From (1), one can note that y is assumed to be independent of ϕ. In general, the damping ratio y_s should not be directly interpreted as corresponding to (1). Indeed, when the sea surface is only partially covered in oil, one introduces a fractional filling factor F, i.e., the ratio of the area covered by a film with respect to the considered total area, and writes the damping ratio y_s as

$$y_s = (1 - F + F/y)^{-1}. \quad (6)$$

In what follows, we will consider a fully covered sea, i.e., $F = 1 \Rightarrow y_s = y$, which is covered by an insoluble film. In Fig. 1, the normalized height spectrum (isotropic part) of a contaminated sea surface $S_{\text{cont}} = M(k)/y$ is plotted versus the wavenumber k for $\{\omega_D = 6$ rad/s, $E_0 = 9$ mN/m$\}$ and $\{\omega_D = 11$ rad/s, $E_0 = 25$ mN/m$\}$. These values were retrieved from experiments that were conducted in the Sicilian Channel and the Gulf of Maine [22]. For comparison, the height spectrum (isotropic part) of a clean sea surface $S_{\text{clean}} = M(k)$ is plotted versus the wavenumber k. The wind speed is $u_{10} = 5$ m/s. As expected, one can observe that the oil film strongly damps the high frequencies, which corresponds to the capillary waves. Moreover, the damping is stronger for $\{\omega_D = 11$ rad/s, $E_0 = 25$ mN/m$\}$ than for $\{\omega_D = 6$ rad/s, $E_0 = 9$ mN/m$\}$.

III. Autocorrelation Function and RMS Slope of a Contaminated Sea Surface

Here, we are interested in the height autocorrelation function W_0, which is equal to the inverse Fourier transform of the height spectrum. For a 1-D surface, using the same parameters as for the height spectrum, the normalized height autocorrelation function is plotted in Fig. 2. That is to say, the three autocorrelation functions are divided by the square of the clean sea water rms height $\sigma_h^{\text{clean}} = 0.161$ m. One can

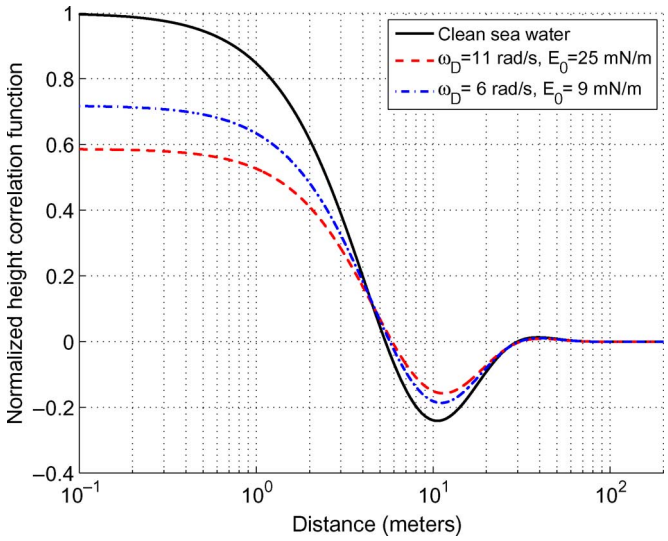

Fig. 2. Normalized height autocorrelation function of clean and contaminated sea surfaces versus the distance. The wind speed is $u_{10} = 5$ m/s.

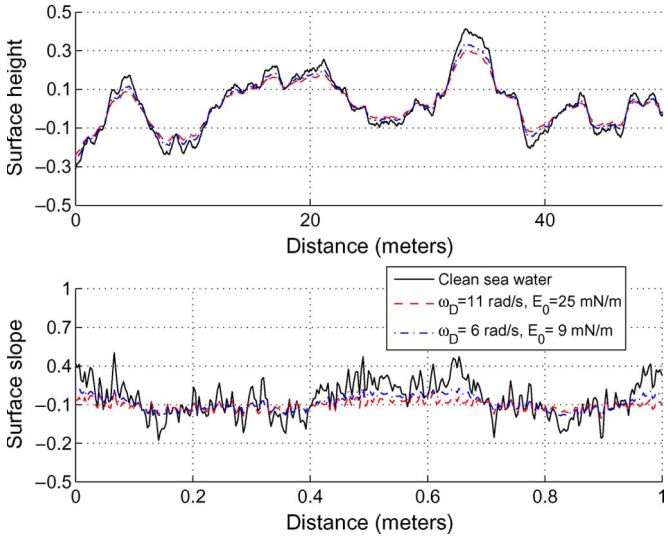

Fig. 3. Surface heights and slopes of a clean sea surface and a sea that is covered in oil. The wind speed is $u_{10} = 5$ m/s.

observe that because of the fact that the capillarity waves are strongly damped by the oil film, the amplitudes of the correlation function for the oil film are smaller than those for a clean sea surface. Moreover, it is smaller for smoother films (i.e., case $\{\omega_D = 11$ rad/s, $E_0 = 25$ mN/m$\}$ is smaller than $\{\omega_D = 6$ rad/s, $E_0 = 9$ mN/m$\}$).

Fig. 3 represents the surface heights and slopes of a realization of a clean sea surface compared to two different types of contaminated seas, with parameters $\{\omega_D = 6$ rad/s, $E_0 = 9$ mN/m$\}$ and $\{\omega_D = 11$ rad/s, $E_0 = 25$ mN/m$\}$. One can observe that the heights are damped and that the slopes are strongly damped for contaminated seas. Moreover, the damping is stronger for $\{\omega_D = 11$ rad/s, $E_0 = 25$ mN/m$\}$ than for $\{\omega_D = 6$ rad/s, $E_0 = 9$ mN/m$\}$, as it was observed in the height spectrum.

With the knowledge of the surface slope spectrum $k^2 S$ of a clean ($k^2 S_{\text{clean}}(k) = k^2 M(k)$) or contaminated ($k^2 S_{\text{cont}}(k) = k^2 M(k)/y$) 1-D sea surface, one can derive its surface rms slope σ_s from the relation

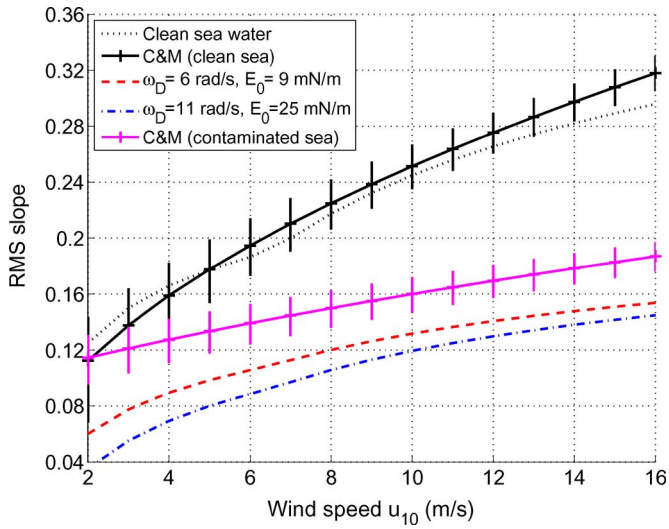

Fig. 4. Surface RMS slope of a 1-D clean sea surface and a 1-D sea that is covered in oil versus the wind speed u_{10}.

$$\sigma_s = \sqrt{\int_0^{+\infty} k^2 S(k)\, dk}. \tag{7}$$

Then, this parameter can be used for modeling the RCS of a contaminated sea with the use of the GOA. Using the same parameters as those stated above, the surface rms slope is plotted in Fig. 4. A comparison is also made with the Cox and Munk [26] experimental model for both clean and contaminated sea surfaces, which is given by the relation (in the upward wind direction)

$$\sigma_s^{\text{clean}} = \sqrt{2} \times \sqrt{3.16 \times 10^{-3}\, u_{12} \pm 2 \times 10^{-3}} \tag{8a}$$

$$\sigma_s^{\text{cont}} = \sqrt{2} \times \sqrt{0.78 \times 10^{-3}\, u_{12} + 5 \times 10^{-3} \pm 4 \times 10^{-3}} \tag{8b}$$

respectively, where u_{12} is the wind speed at 12.5 m above the sea. Here, the rms slopes of the Cox and Munk experimental model, which are defined for 2-D surfaces, are multiplied by $\sqrt{2}$ to be consistent with the rms slope in (7) defined from the spectrum of 1-D surfaces. Let us note that the Cox and Munk rms slope of the contaminated sea was obtained from 200 gal of oil poured out, and the slick was 2000 ft $\times$ 200 ft. This corresponds to an oil layer thickness $H \simeq 20$ μm. One can observe in Fig. 4 a good agreement for the rms slope of a clean sea surface between the Elfouhaily height spectrum model and the Cox and Munk model (which is denoted as "C&M" in the legend). Moreover, there is also a rather good qualitative agreement between the two contaminated films with the Lombardini *et al.* model and the Cox and Munk model for contaminated seas. Nevertheless, differences remain between the two cases. This can be attributed to the fact that the Lombardini *et al.* model [22] is independent of the oil layer thickness and is only valid for thick oil films, that is to say, on the order of a hundred micrometers to a millimeter (by comparison with the Cox and

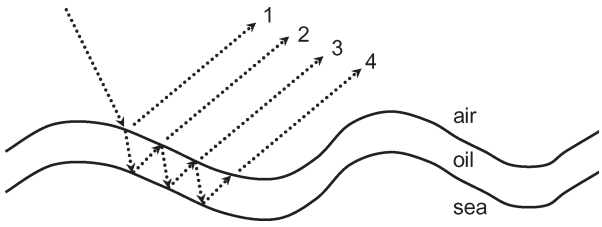

Fig. 5. Multiple scattering from the contaminated sea: representation of the first four orders.

Munk experimental model, which was obtained from slicks of around 20 μm). Indeed, the rms slope decreases as the layer thickness increases.

Then, in Section IV, the impact of the modified height spectrum for contaminated seas (compared to clean seas) on the RCS is studied.

IV. Impact on the RCS

Let us have a look at the modification of the RCS from the contaminated sea, in comparison with the RCS of a clean sea surface. First, a benchmark numerical method is used.

The benchmark numerical method used here is the PILE method combined with the FB method. A detailed explanation of the PILE method can be found in [16], and literature about the FB method can be found in [20]. It is worth noting that the FB method with a novel spectral acceleration [27]–[29] devoted to a layer exists [30]; however, this method does not converge for a layer as thin as the one in our study (0.1λ or 0.01λ). One of the advantages of the PILE method is its ability to rigourously calculate the contribution of each scattering from the rough layer (see Fig. 5). Thus, the first order represents the scattering from only the air–oil interface of the contaminated sea, whereas the second order represents the scattering from the layer where the incident wave undergoes one reflection inside the dielectric layer, and so on for the higher orders. Then, the order of the PILE method corresponds to the order of scattering from the rough layer.

The numerical simulations were conducted at a frequency $f = 3$ GHz, for a wind speed $u_{10} = 5$ m/s, with an insoluble oil film of parameters $\{\omega_D = 6$ rad/s, $E_0 = 9$ mN/m$\}$ and mean thickness $\bar{H} = \{0.1, 0.01\}\lambda = \{10, 1\}$ mm. The results are given here for horizontal (H) and vertical (V) polarizations. At $f = 3$ GHz, the sea surface relative permittivity is equal to $\epsilon_r^{\text{sea}} = 70.4 + i40.6$ [17], and the oil relative permittivity is taken as $\epsilon_r^{\text{oil}} = 2.25 + i0.01$ [18], [19], [31]. Let us note that for various types of oil, the real (ϵ_r') and imaginary (ϵ_r'') parts of the relative permittivity vary very slightly, i.e., approximately $2.15 \leq \epsilon_r' \leq 2.25$ and $0 \leq \epsilon_r' \leq 0.02$, respectively. However, this does not have a significant influence on the scattering coefficient. The same conclusion can be drawn for the temperature variability [32].

The parameters of the numerical method are the sampling step $\Delta x = \lambda/10$, with a total surface length $L = 25$ m (250λ), which makes $n_i = 2500$ samples per interface. The incident beam is a Thorsos wave, with a tapering parameter $g = L/6$. The PILE method, as well as the FB method, which was used to speed up the PILE method, was used at order 6. A Monte Carlo average was performed over 50 realizations to obtain the bistatic incoherent scattering coefficient σ.

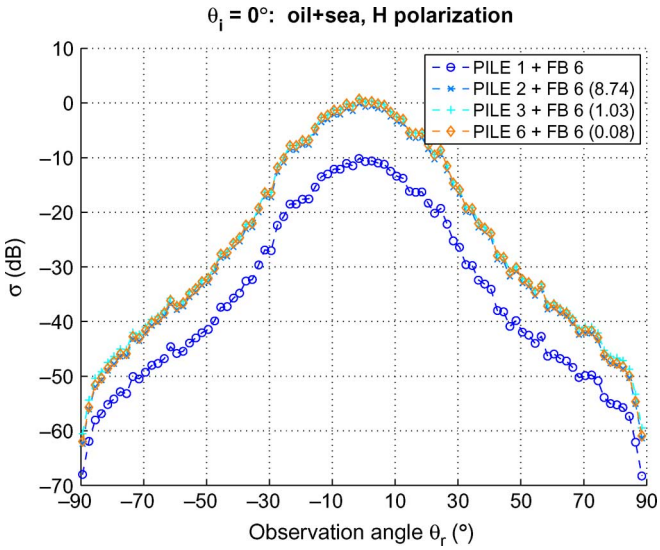

Fig. 6. Bistatic scattering coefficients of a contaminated sea for $f = 3$ GHz and $\theta_i = 0°$, with $\bar{H} = 10$ mm: cumulated orders 1, 2, 3, 6 of the benchmark (PILE+FB) numerical method. The wind speed is $u_{10} = 5$ m/s.

A. Numerical Results of FB and PILE+FB

For a clean sea surface, the numerical results of the FB method (not presented here) showed that the FB method converges as soon as order 2 for V polarization and at order 6 for H polarization. Indeed, for V polarization, the absolute mean difference between the scattering coefficients at orders 2 and 3 equals 2×10^{-4} dB, and for H polarization, the absolute mean difference between the scattering coefficients at orders 5 and 6 equals 4×10^{-3} dB. Then, in what follows, in all cases, the FB method will be used at order 6.

For a contaminated sea surface, the numerical results of the PILE method combined with the FB method (at order 6) are presented in Fig. 6 for a mean layer thickness $\bar{H} = 0.1\lambda = 10$ mm. Let us note that this value of layer thickness is not a representation of the typical thicknesses of oil slicks (the typical thickness is inferior to or on the order of 1 mm). Nevertheless, for thinner layers, the numerical method has problems of convergence for V polarization. It is the numerical problem of convergence that limits the applicability of the method for very thin layers (more precisely, the problem comes from bad conditioning of the integral methods on which the PILE method is based). Then, we will concentrate on thickness $\bar{H} = 0.1\lambda = 10$ mm by considering both polarizations. Nevertheless, we will further see that the numerical results are qualitatively and quantitatively very similar for the two polarizations. Thus, for thinner layers, we will present results only for H polarization.

The numerical results present the cumulated orders 1, 2, 3, 6 of the PILE method, which correspond to the orders 1, 2, 3, 6 of scattering from the layer (see Fig. 6). In the legend, the value inside the parentheses represents the absolute difference between the mean cumulated scattering coefficients of order n and order $n-1$, with n being the considered cumulated order. The numerical results show that, contrary to the second order,

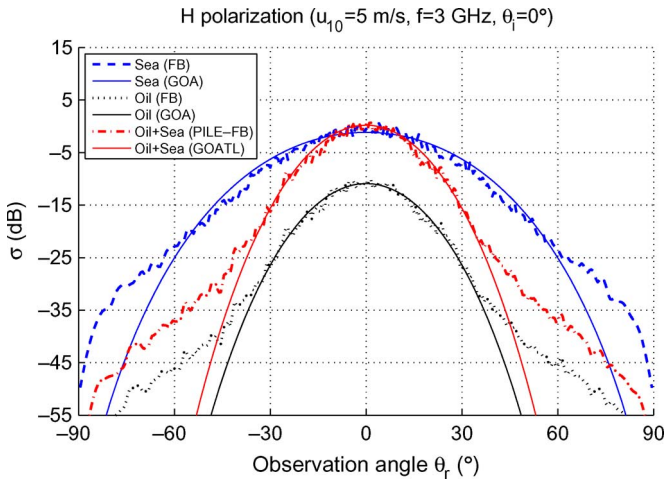

Fig. 7. Bistatic scattering coefficients of clean and contaminated seas for $f = 3$ GHz and $\theta_i = 0°$, with $\bar{H} = 10$ mm: comparison between the benchmark numerical method and the GOA. The wind speed is $u_{10} = 5$ m/s.

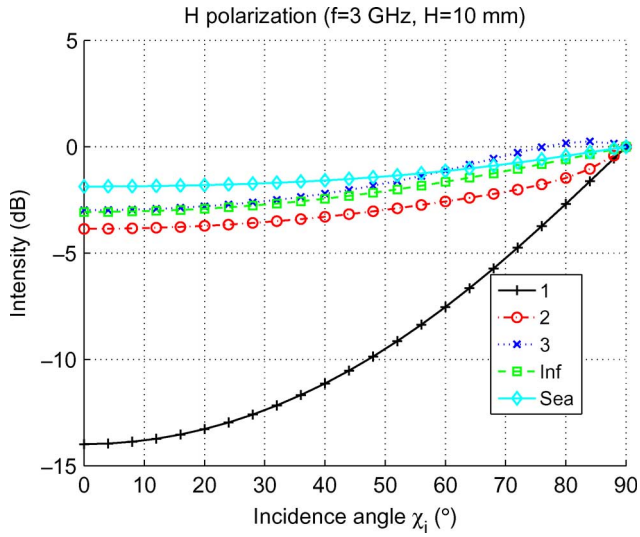

Fig. 8. Square modulus of the equivalent reflection coefficient (with $f = 3$ GHz and $\bar{H} = 10$ mm) for H polarization and comparison with that of a clean sea surface. The first three orders of the equivalent reflection coefficient are also plotted for comparison.

the first order of the PILE method has a low contribution to the total scattering coefficient. Indeed, the second order has a very strong contribution, such that the higher orders have a weak contribution to the total scattering coefficient.

Now, the benchmark numerical method is compared to an asymptotic approach. First, for a clean sea surface and for the first order of the scattering coefficient of the contaminated sea (corresponding to the scattering from the air–oil interface), a basic asymptotic method will be used. Then, a new semiempirical model for a thin layer of oil is presented: first, based on the GOA and, second, based on the SSA-1.

B. Comparison of the Benchmark Method With GOA

Fig. 7 represents the bistatic scattering coefficients of clean and contaminated seas for H polarization (similar conclusions can be drawn for V polarization). For a clean sea surface, the benchmark numerical results, which are plotted in dashed blue line, are compared with the GOA, which are plotted in solid blue line. One can observe a good agreement between the two curves around the specular direction, for $\theta_r \in [-30°; +30°]$ approximately. This is because, for low incidence angles and around the specular direction, only the gravity waves of the sea spectrum contribute to the scattering coefficient. For a contaminated sea, the first order of the scattering coefficient, corresponding to the scattering from the air–oil interface, is plotted in dotted black line for the numerical method (which corresponds to order 1 of the PILE+FB method) and in solid black line for the GOA. One also observes a good agreement around the specular direction, for $\theta_r \in [-40°; +40°]$ approximately. This is because, for low incidence angles and around the specular direction, only the gravity waves of the sea spectrum contribute to the scattering coefficient. Here, the range of validity over θ_r is larger than that of a clean sea surface, as the oil film damps the capillarity waves of the surface spectrum.

The total scattering coefficient of a contaminated sea is plotted in red dash–dotted line for the numerical method. By comparison with the first order, the scattering coefficient is higher for all scattering angles θ_r. It was calculated that for the typical configuration presented here, the second-order scattering coefficient (corresponding to one reflection inside the oil layer) of the benchmark method mainly contributes to the total scattering coefficient. This explains why no significant oscillation in the scattering coefficient occurs, which would be due to the interference between the successive reflections inside the layer. Moreover, it is close to the scattering coefficient of a clean sea surface around the specular direction (in the specular direction, the difference is about 1.4 dB). This is because the oil film is rather transparent (relative permittivity close to unity). The differences can be attributed to the differences in the surface spectrum. Indeed, a sea that is covered in oil has a lower rms slope. Consequently, the energy distribution of the scattering coefficient is more concentrated around the specular direction for a contaminated sea than for a clean sea. The maximum, which occurs in the specular direction, is then higher, and the scattering coefficient decreases more rapidly away from the specular direction for the contaminated sea than for the clean sea.

To physically explain the behavior of the curves in Fig. 7 and to build a new semiempirical model, the plane slab case is studied. Because the oil layer is thin ($\bar{H} = 0.1\lambda = 10$ mm here), for low incidence angles, the interfaces that induce the multiple reflected waves from the oil layer can be considered as locally plane parallel interfaces. Then, the two interfaces can be substituted with one interface by replacing the Fresnel reflection coefficient of the upper air–oil interface $r_{12}(\chi_i)$, where $\chi_i = -(\theta_r - \theta_i)/2$ is the local incidence angle, with the equivalent reflection coefficient $r_{\text{eq}}(\chi_i)$. The latter is given by the relation

$$r_{\text{eq}}(\chi_i) = \frac{r_{12}(\chi_i) + r_{23}(\chi_m)\, e^{-j\Delta\phi}}{1 + r_{12}(\chi_i) r_{23}(\chi_m)\, e^{-j\Delta\phi}} \tag{9}$$

where $r_{23}(\chi_m)$ is the Fresnel reflection coefficient of the lower oil–sea interface, with χ_m being the local incidence angle given by the Snell–Descartes law $\sqrt{\epsilon_{r1}} \sin \chi_i = \sqrt{\epsilon_{r2}} \sin \chi_m$. $\Delta\phi$ is

the phase difference between the first- and second-order reflected fields, which is given by the relation $\Delta\phi = 2k_2\bar{H}\cos\chi_m$, with k_2 being the wavenumber inside the oil film.

Fig. 8 represents a comparison between the square modulus of the reflection coefficient of a clean sea surface, which is plotted in cyan line with rhombuses, with that of a contaminated sea, which is plotted in green line with squares. The frequency $f = 3$ GHz, the mean layer thickness $\bar{H} = 10$ mm, and H polarization is considered. The first three orders of the equivalent reflection coefficient of the contaminated sea, which are defined as

$$r_{\mathrm{eq},1}(\chi_i) = r_{12}(\chi_i) \tag{10}$$

$$r_{\mathrm{eq},p}(\chi_i) = r_{12}(\chi_i) + t_{12}(\chi_i)t_{21}(\chi_m) \times \sum_{k=0}^{p-2} r_{23}^{k+1}(\chi_m) r_{21}^{k}(\chi_m)\, e^{-j(k+1)\Delta\phi} \tag{11}$$

where $p = \{2, 3\}$, and t_{12} and t_{21} are the Fresnel transmission coefficients of the air–oil interface, are also plotted for comparison: the first order then corresponds to the air–oil interface only. First, one can observe that the results of the contaminated sea are smaller than those of the clean sea and that the difference between the two curves is relatively small (inferior to 1.2 dB) for all incidence angles χ_i. This partly explains in Fig. 7 the small difference in the scattering coefficients in the specular direction (equal to approximately 1.4 dB). Nevertheless, the scattering coefficient of the contaminated sea is higher than that of the clean sea. Indeed, the difference is also due to the difference in the rms slopes: $\sigma_s^{\mathrm{clean}} \simeq 0.169$ for a clean sea and $\sigma_s^{\mathrm{cont}} \simeq 0.098$ for a contaminated sea. Thus, the difference in the specular direction between the contaminated and clean seas is given by the relation $|r_{\mathrm{eq}}(0)/r_{12}(0)|^2 \times \sigma_s^{\mathrm{clean}}/\sigma_s^{\mathrm{cont}}$, which equals 1.4 dB. Second, the difference between the air–oil interface, which is plotted in black line with plus signs, and the contaminated sea explains the difference in the scattering coefficients. Indeed, for a local incidence angle $\chi_i = 0$, corresponding to $\theta_i = 0$ to $\theta_r = 0$, the difference is the highest. Then, for higher values of χ_i (or $-\chi_i$), corresponding to increasing $|\theta_r|$, the reflection coefficient of the air–oil interface significantly increases (contrary to the contaminated sea), such that the difference between the two curves decreases. In Fig. 7, the same phenomenon is observed for the scattering coefficients.

Thus, based on the GOA, we introduce a new semiempirical GOATL (TL for thin layer) model, which takes the oil layer into account by replacing $r_{12}(\chi_i)$ for the air–oil interface with $r_{\mathrm{eq}}(\chi_i)$. The corresponding curve is plotted in Fig. 7 in solid red line. Then, one can observe a good agreement between the benchmark numerical method, which is plotted in dash–dotted red line, and our new semiempirical model around the specular direction, for $\theta_r \in [-40°; +40°]$ approximately. As for the first-order scattering coefficient, this is because, for low incidence angles and around the specular direction, only the gravity waves of the sea spectrum contribute to the scattering coefficient. The range of validity over θ_r is larger than that of a clean sea surface, as the oil film damps the capillarity waves of the surface spectrum. In Section IV-C, the benchmark numerical method is compared to the SSA-1, from which a new semiempirical model for the contaminated sea is also derived.

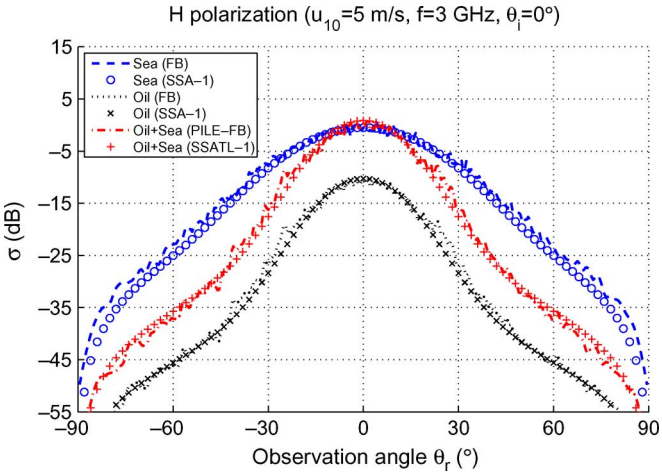

Fig. 9. Bistatic scattering coefficients of clean and contaminated seas for $f = 3$ GHz and $\theta_i = 0°$, with $\bar{H} = 10$ mm: comparison between the benchmark numerical method and the SSA-1. The wind speed is $u_{10} = 5$ m/s.

C. Comparison of the Benchmark Method With SSA-1

From the results of the GOA in comparison to the benchmark model, using the same way, one can derive results based on the SSA [7]. Indeed, the SSA is an approximate model that is well adapted to scattering from sea surfaces [8], [9], [33], as it takes the gravity waves, as well as the capillarity waves, into account, on the condition of small surface slopes compared to the incident and scattered beam slopes. Here, results will be presented for the first-order contribution of the SSA only (which is denoted as SSA-1). Then, the SSA-1 is applied to a clean sea surface, as well as to the air–oil interface (corresponding to the first-order scattering coefficient of the contaminated sea), with the knowledge of the considered surface autocorrelation function. For the whole scattering coefficient of a contaminated sea, the same way as for the GOA is used. That is to say, the new SSATL-1 (TL for thin layer) model, corresponding to the contaminated sea, is obtained from the SSA-1 from the air–oil interface, multiplied by the ratio $|r_{\mathrm{eq}}(\chi_i)/r_{12}(\chi_i)|^2$.

Then, Fig. 9 presents results of the SSATL-1 in comparison with the benchmark numerical method. For the SSA-1, the clean sea is represented with blue circles, the air–oil interface with black plus signs, and the contaminated sea with red crosses. For the clean sea surface, one can observe a very good agreement with the benchmark method for scattering angles $\theta_r \in [-50°; +50°]$ approximately. For higher scattering angles, the SSA-1 underestimates the scattering coefficient. This can be attributed to the fact that only the SSA-1 is considered here. Indeed, in H polarization and for highly conducting media such as a sea surface, the scattering coefficient is very sensitive to the Bragg modulation. This is confirmed by the results of the air–oil interface (the oil is a weakly conducting medium), which coincide very well with the benchmark method for all scattering angles. In Fig. 10, the results for V polarization show good agreement for the sea surface for all scattering angles.

For the scattering coefficient of the contaminated sea, one can observe a very good agreement between the new SSATL-1 and the benchmark models for both H and V polarizations and for all scattering angles. This allows us to validate the new

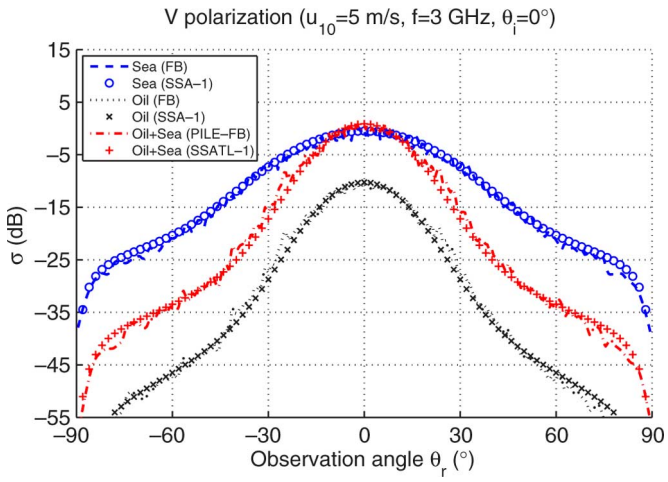

Fig. 10. Same simulations as in Fig. 9, but for V polarization.

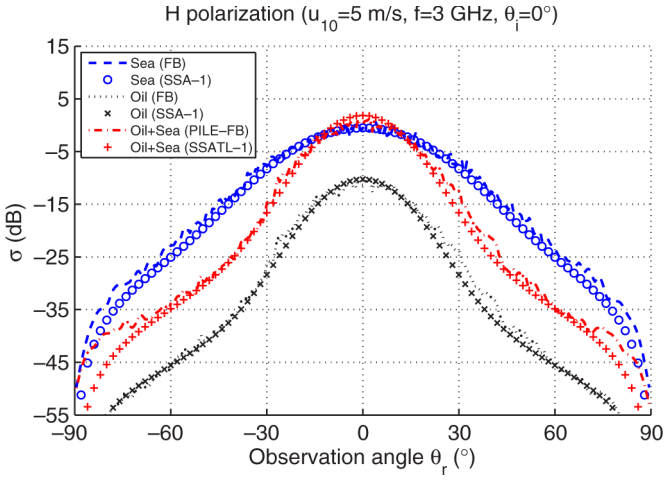

Fig. 11. Same simulations as in Fig. 9, but with a mean layer thickness $\bar{H} = 1$ mm.

semiempirical model presented here for this kind of configuration (i.e., for thin layers $\bar{H} \lesssim 10$ mm), which considers locally plane parallel interfaces and replaces the Fresnel reflection coefficient of the upper interface $r_{12}(\chi_i)$ with the equivalent reflection coefficient $r_{\text{eq}}(\chi_i)$.

Now, for a more realistic representation of the oil layer, let us have a look at the scattering coefficient for a mean layer thickness $\bar{H} = 0.01\lambda = 1$ mm. Fig. 11 presents results for an incidence angle $\theta_i = 0°$. As expected, the results of the SSATL-1 are in good agreement with the benchmark PILE+FB method for moderate scattering angles θ_r. Results in Fig. 12 for $\theta_i = -20°$ show a good agreement for moderate θ_r. Then, the new semiempirical model presented here can be applied for thin layers, and its association with the SSA-1, namely the SSATL-1, gives results in agreement with the benchmark method for moderate scattering angles θ_r.

As a final remark, if we consider partial oil coverage (i.e., $0 \leq F < 1$), the numerical results will differ, depending on the value of F. Indeed, in general, the total scattering coefficient results as a first approximation from the summation of that of the sea that is covered in oil and that of the clean sea, multiplied by F and $1 - F$, respectively. Thus, for F close to one, the

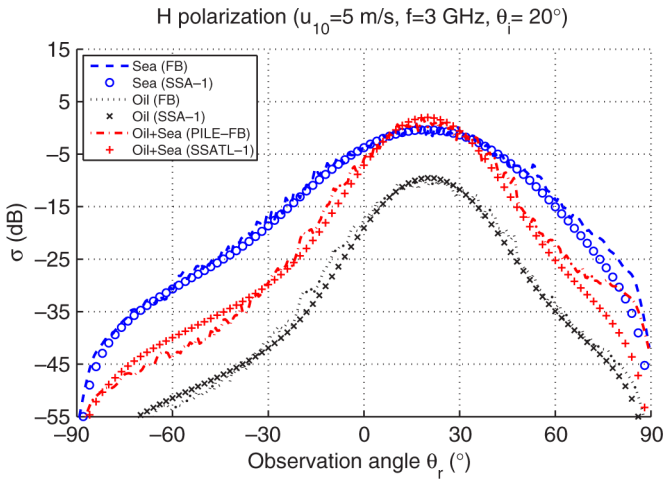

Fig. 12. Same simulations as in Fig. 11, but for $\theta_i = -20°$.

results do not change significantly from a totally covered sea. On the other hand, for F close to zero, the results are close to the ones with a clean sea surface. In the transition zone, as F decreases, the results of the scattering coefficient gradually move from a totally covered sea to a clean sea.

V. Conclusion

The influence of the height spectrum of a contaminated sea, by comparison with a clean sea, on the scattering coefficient has been studied. It was found that the oil slick damps the capillarity waves of the surface spectrum, implying a lower surface rms slope. The bistatic RCSs of a clean sea surface and a contaminated sea were then simulated. Numerical results from a benchmark method, called PILE+FB, were presented. Then, a new semiempirical model was derived for the case of thin layers by considering locally plane parallel interfaces. First, it was based on the GOA, and second, it was extended to the SSA-1, which was called SSATL-1: a good agreement was then found with the benchmark method for moderate scattering angles. Thus, this new simple model has allowed fast prediction of the bistatic RCS of a contaminated sea.

Acknowledgment

The authors would like ot thank the anonymous reviewers for their useful comments and suggestions.

References

[1] D. Thompson, T. Elfouhaily, and J. Garrison, "An improved geometrical optics model for bistatic GPS scattering from the ocean surface," *IEEE Trans. Geosci. Remote Sens.*, vol. 43, no. 12, pp. 2810–2821, Dec. 2005.

[2] L. Tsang and J. Kong, *Scattering of Electromagnetic Waves*, vol. III. New York: Wiley, 2001.

[3] J. Ogilvy, *Theory of Wave Scattering From Random Surfaces*. Philadelphia, PA: Inst. Phys. Publishing, 1991.

[4] F. Bass and I. Fuks, *Wave Scattering From Statistically Rough Surfaces*. Oxford, U.K.: Pergamon, 1978.

[5] P. Beckmann and A. Spizzichino, *The Scattering of Electromagnetic Waves From Rough Surfaces*. Oxford, U.K.: Pergamon, 1963.

[6] J. Johnson, "An efficient two-scale model for the computation of thermal emission and atmospheric reflection from the sea surface," *IEEE Trans. Geosci. Remote Sens.*, vol. 44, no. 3, pp. 560–568, Mar. 2006.

[7] A. Voronovich, *Wave Scattering From Rough Surfaces*, 2nd ed. Berlin, Germany: Springer-Verlag, 1999.
[8] A. Voronovich and V. Zavorotny, "Theoretical model for scattering of radar signals in K_u- and C-bands from a rough sea surface with breaking waves," *Waves Random Media*, vol. 11, no. 3, pp. 247–269, 2001.
[9] S. T. McDaniel, "Microwave backscatter from non-Gaussian seas," *IEEE Trans. Geosci. Remote Sens.*, vol. 41, no. 1, pp. 811–817, Jan. 2003.
[10] C. Bourlier, "Azimuthal harmonic coefficients of the microwave backscattering from a non-Gaussian ocean surface with the first-order SSA model," *IEEE Trans. Geosci. Remote Sens.*, vol. 42, no. 11, pp. 2600–2611, Nov. 2004.
[11] J. Johnson, "A study of ocean-like surface thermal emission and reflection using Voronovich's small slope approximation," *IEEE Trans. Geosci. Remote Sens.*, vol. 43, no. 2, pp. 306–314, Feb. 2005.
[12] T. Elfouhaily, S. Guignard, R. Awadallah, and D. Thompson, "Local and non-local curvature approximation: A new asymptotic theory for wave scattering," *Waves Random Media*, vol. 13, no. 4, pp. 321–337, Oct. 2003.
[13] J. Álvarez Pérez, "An extension of the IEM/IEMM surface scattering model," *Waves Random Media*, vol. 11, no. 3, pp. 307–329, Jul. 2001.
[14] T. Elfouhaily and C.-A. Guérin, "A critical survey of approximate scattering wave theories from random rough surfaces," *Waves Random Media*, vol. 14, no. 4, pp. R1–R40, Oct. 2004.
[15] L. Tsang, J. A. Kong, K. H. Ding, and C. O. Ao, *Scattering of Electromagnetic Waves*, vol. II. New York: Wiley, 2001.
[16] N. Déchamps, N. de Beaucoudrey, C. Bourlier, and S. Toutain, "Fast numerical method for electromagnetic scattering by rough layered interfaces: Propagation-inside-layer expansion method," *J. Opt. Soc. Amer. A, Opt. Image Sci.*, vol. 23, no. 2, pp. 359–369, Feb. 2006.
[17] W. Ellison, A. Balana, G. Delbos, K. Lamkaouchi, L. Eymard, C. Guillou, and C. Prigent, "New permittivity measurements of seawater," *Radio Sci.*, vol. 33, no. 3, pp. 639–648, 1998.
[18] F. Ulaby, R. Moore, and A. Fung, *Microwave Remote Sensing: Active and Passive*, vol. 3. Norwood, MA: Artech House, 1986.
[19] T. Friizo, Y. Schildberg, O. Rambeau, T. Tjomsland, H. Fordedal, and J. Sjoblom, "Complex permittivity of crude oils and solutions of heavy crude oils fractions," *J. Dispers. Sci. Technol.*, vol. 19, no. 1, pp. 93–126, 1998.
[20] A. Iodice, "Forward–backward method for scattering from dielectric rough surfaces," *IEEE Trans. Antennas Propag.*, vol. 50, no. 7, pp. 901–911, Jul. 2002.
[21] T. Elfouhaily, B. Chapron, K. Katsaros, and D. Vandemark, "A unified directional spectrum for long and short wind-driven waves," *J. Geophys. Res.*, vol. 102, no. C7, pp. 781–796, Jul. 1997.
[22] P. Lombardini, B. Fiscella, P. Trivero, C. Cappa, and W. Garrett, "Modulation of the spectra of short gravity waves by sea surface films: Slick detection and characterization with a microwave probe," *J. Atmos. Ocean. Technol.*, vol. 6, no. 6, pp. 882–890, Dec. 1989.
[23] N. Skou, "Microwave radiometry for oil pollution monitoring, measurements, and systems," *IEEE Trans. Geosci. Remote Sens.*, vol. GE-24, no. 3, pp. 360–367, May 1986.
[24] E. Brown, O. McMahon, T. Murphy, G. Hogan, G. Daniels, and G. Hover, "Wide-band radiometry for remote sensing of oil films on water," *IEEE Trans. Microw. Theory Tech.*, vol. 46, no. 12, pp. 1989–1996, Dec. 1998.
[25] K. Lamkaouchi, "Water: A dielectric standard. Permittivity of water-petrol mixtures at microwave frequencies," Ph.D. dissertation, Bordeaux I Univ., Bordeaux, France, Jun. 1992. in French.
[26] C. Cox and W. Munk, "Measurement of the roughness of the sea surface from photographs of the sun's glitter," *J. Opt. Soc. Amer.*, vol. 44, no. 11, pp. 838–850, Nov. 1954.
[27] H.-T. Chou and J. Johnson, "A novel acceleration algorithm for the computation of scattering from rough surfaces with the forward–backward method," *Radio Sci.*, vol. 33, no. 5, pp. 1277–1287, 1998.
[28] H.-T. Chou and J. Johnson, "Formulation of forward-backward method using novel spectral acceleration for the modeling of scattering from impedance rough surfaces," *IEEE Trans. Geosci. Remote Sens.*, vol. 38, no. 1, pp. 605–607, Jan. 2000.
[29] D. Torrungrueng and J. Johnson, "Some issues related to the novel spectral acceleration method for the fast computation of radiation/scattering from one-dimensional extremely large scale quasi-planar structures," *Radio Sci.*, vol. 37, no. 2, p. 1019, 2002.
[30] C. Moss, T. Grzegorczyk, H. Han, and J. Kong, "Forward-backward method with spectral acceleration for scattering from layered rough surfaces," *IEEE Trans. Antennas Propag.*, vol. 54, no. 10, pp. 2917–2929, 2006.
[31] K. Folgero, "Bilinear calibration of coaxial transmission/reflection cells for permittivity measurement of low-loss liquids," *Meas. Sci. Technol.*, vol. 7, no. 9, pp. 1260–1269, Sep. 1996.
[32] T. Friiso and T. Tjomsland, "Monitoring of density changes in low-permittivity liquids by microwave-permittivity measurements with an open-ended probe," *Meas. Sci. Technol.*, vol. 8, no. 11, pp. 1295–1305, Nov. 1997.
[33] C. Bourlier, N. Déchamps, and G. Berginc, "Comparison of asymptotic backscattering models (SSA, WCA, and LCA) from one-dimensional Gaussian ocean-like surfaces," *IEEE Trans. Antennas Propag.*, vol. 53, no. 5, pp. 1640–1652, May 2005.

Nicolas Pinel was born in Saint-Brieuc, France, in 1980. He received the Engineering degree and M.S. degrees in electronics and electrical engineering both in 2003 and the Ph.D. degree in 2006 from the University of Nantes, Nantes, France.

He is currently with the Radar Team, Institut de Recherche en Electrotechnique et Electronique de Nantes Atlantique (IREENA) Laboratory, Ecole Polytechnique de l'Université d Nantes (EPUN), University of Nantes, working on asymptotic methods of electromagnetic wave scattering from stacks of rough interfaces.

Nicolas Déchamps was born in Provins, France, in 1977. He received the B.Eng. degree from the Ecole Centrale de Nantes (ECN), Nantes, France, in 2001, the M.Sc. degree in automation and applied computer science from the Communications and Cybernetic Research Institute of Nantes (IRCCyN), Nantes, in 2001, and the Ph.D. degree in physics from the University of Nantes, Nantes, in 2004.

After a postdoctoral position at the Pulp and Paper Center at the University of Toronto, Toronto, ON, Canada, where he worked on optical properties of paper, he joined the Radar Team, Institut de Recherche en Electrotechnique et Electronique de Nantes Atlantique (IREENA) Laboratory, Ecole Polytechnique de l'Université d Nantes (EPUN), University of Nantes, as a Research Associate in 2006. His research interest includes fast methods for numerical simulations of scattering from multilayers separated by rough interfaces and analytical modeling of paper gloss.

Christophe Bourlier (M'05–A'05) was born in La Flèche, France, on July 6, 1971. He received the M.S. degree in electronics from the University of Rennes, Rennes, France, in 1995 and the Ph.D. degree from the Système Electronique et Informatique Laboratory (SEI), Nantes, France, in 1999.

While at the University of Rennes, he was with the Laboratory of Radiocommunication, where he worked on antenna coupling in the VHF–HF band. He is currently with the Institut de Recherche en Electrotechnique et Electronique de Nantes Atlantique (IREENA) Laboratory and the Radar Team, Polytech'Nantes, University of Nantes, Nantes, France, as a National Center for Scientific Research (CNRS) Assistant Researcher, working on electromagnetic wave scattering from rough surfaces and objects for remote sensing applications. He is the author of more than 80 journal articles and conference proceedings.